Open Access

Advances in Environmental and Engineering Research

LIDSEN Publishing Inc.

Original Research

Cellular Photosynthetic Pigment and Structural Change in *Festuca arundinacea* (Tall Fescue) after Exposure to Acute and Chronic Chromium and Copper Stress

Danae M. Maes [1, †], August Finke [2, †], Chuck R. Smallwood [2], J. Bryce Ricken [2], Jerilyn A. Timlin [1], Anne M. Ruffing [2, *]

1. Sandia National Laboratories: Computational Biology & Biophysics, P.O. Box 5800, MS 0895, Albuquerque, NM 87185, USA; E-Mails: dmaes@sandia.gov; jatimli@sandia.gov
2. Sandia National Laboratories: Molecular and Microbiology, P.O. Box 5800, MS 1413, Albuquerque, NM 87185, USA; E-Mails: afinke@sandia.gov; crsmall@sandia.gov; bricken@sandia.gov; aruffin@sandia.gov

† These authors contributed equally to this work.

* **Correspondence:** Anne M. Ruffing; E-Mail: aruffin@sandia.gov

Special Issue: Metal Pollution in the Environment

Adv Environ Eng Res
2022, volume 3, issue 2
doi:10.21926/aeer.2202025

Received: April 11, 2022
Accepted: June 01, 2022
Published: June 14, 2022

Abstract

Expanded industrial globalization has resulted in the release of high concentrations of heavy metals into environmental water sources and soils. Phytoremediation may help to remove these heavy metals from contaminated soils. Tall fescue (*Festuca arundinacea Shreb.*) exhibits phytoremediation potential due to its endurance and high stress tolerances. Here, we report photochemical and structural responses in tall fescue to acute and chronic doses of heavy metals, copper (Cu) and hexavalent chromium (Cr(VI)). Visual signs of stress and decreased photosynthetic yield measurements were detected for both the acute and chronic exposures. To gain insight into stress responses at the cellular level, structural and pigment changes in tall fescue in response to Cu and Cr(VI) stress were assessed with brightfield and confocal fluorescence imaging. While brightfield images showed qualitative changes in plant tissue structure, the quantification of changes were not statistically significant due to high variability

between leaf blades. Fluorescence imaging confirmed decreasing total chlorophyll content in tall fescue cross-sections in response to Cr(VI) and Cu exposure. To spectrally separate the closely related chlorophyll pigments (Chl-a, Chl-b, and Chl in photosystem I) and visualize their relative localizations within the plant tissue, hyperspectral confocal fluorescence microscopy was conducted with multivariate curve resolution (MCR) analysis of the data. These results determined that Chl-a and Chl-b were more significantly reduced than Chl associated with photosystem I. Additionally, a new spectral component was identified. A broad autofluorescence (AF) feature appeared in the late stress response of both acute and chronically exposed tall fescue and was localized in globular bodies. While the identity of the broad AF feature remains to be identified, we hypothesize that it may be associated with degraded chlorophyll components in autophagic bodies. If confirmed, this would indicate that autophagy is a stress response to heavy metal exposure in tall fescue.

Keywords
Metal stress; plant stress; hyperspectral imaging; confocal fluorescence microscopy; brightfield microscopy

1. Introduction

Expansion in global industrialization has resulted in increased pollution of metal ion contaminates in aquatic and terrestrial environments [1-4]. Heavy metal contaminant sources include mines and chemical plants, which are likely to introduce metal ions to the environment through wastewater, chemical discard, and refuse. The Hanford site, an early nuclear production plant, caused toxic and radioactive metal contamination to the local environment. One of the most notable contaminants released was chromate [5]. Hexavalent chromium, or Cr(VI), is a highly toxic and water-soluble metal ion, resulting in rapid dispersal into the groundwater [6, 7]. Chromium has a wide variety of industrialization applications and uses including leather tanning, metal finishing, steel production, catalyst applications, electroplating, electricity generation, refining, and more [6, 8]. While Cr(VI) is naturally found in the environment at low concentrations, usually ranging from 10-50 mg/kg soil [9], anthropogenic activities such as ore smelting, industrial fabrication and manufacturing, sewage and waste dumping raise Cr(VI) concentrations in polluted regions [10]. These rising rates could have negative consequences to the exposed biomes resulting in loss of vegetation for ecological homeostasis.

Copper (Cu) is another common metal pollutant that can have negative ecological effects. It is usually found in the environment at trace concentrations ranging from 2-100 mg/kg depending on geographical location [11, 12]. Like Cr(VI), it can be found in much higher and more dangerous concentrations, up to several thousand mg/kg near mines and timber treatment facilities [13, 14]. Farmland, in which Cu based pesticides are used, may have Cu levels ranging from 100-1500 mg/kg [15]. Understanding the impact these metal contaminants have on the environment is important for informing regulatory policy and guiding remediation efforts.

Previous studies have been conducted to determine the effect of heavy metals in plants. Heavy metal ions, such as Cr(VI), Cu, zinc, cadmium, nickel, and more, have been found to cause oxidative

stress in plants, which disturbs cellular homeostasis and other biological functions and activities [16]. This leads to cellular damage and impacts overall plant health and physiology [16]. Plants exposed to heavy metals have varied responses, including slowed growth and germination, loss of turgor pressure, chlorosis, necrosis, and impaired photosynthetic apparatuses [17]. The effects of Cr(VI) have been extensively studied on terrestrial and aquatic plants. Cr(VI) accumulation in *Nymphaea alba* L. has been shown to lead to reduced chlorophyll levels by inhibiting chlorophyll biosynthesis [18]. Soybean (*Glycine max* L. Merr.) and water lettuce (*Pistia stratiotes* L.) both exhibited reduced levels of chlorophyll, carotenoids, proteins, amino acids, and enzymatic activities at Cr(VI) concentrations of 300 mg/L and above [19]. Other studies have confirmed that plants exposed to increased Cr(VI) levels display inhibited growth, leaf chlorosis, nutrient imbalances, and root and leaf damage [20-23]. While Cu can be beneficial to plants in small amounts [24], excess Cu is cytotoxic, resulting in stress and damage to plant health [16]. Characteristics of Cu stress in plants include slowed growth and leaf chlorosis [25]. While these studies have characterized whole plant and leaf-level physiological, metabolic, and genetic responses of plants to Cr(VI) and Cu stress, few studies have investigated spatial changes in pigment localization at the cellular level.

Plants utilize a variety of pigments such as chlorophylls and carotenoids which serve to harvest light and transform it into energy. Most of these pigments have endogenous fluorescence emissions that are strongly simliar to each other to promote efficient energy transfer. Hyperspectral confocal fluorescence microscopy (HCFM) along with multivariate curve resolution (MCR) data analysis, allows for the detection of fluorescence signatures associated with photosynthetic pigments such as chlorophylls and carotenoids and maps their location within living organisms, despite their significant degree of spectral overlap [26, 27]. MCR analysis of the hyperspectral data identifies the pure component spectra associated with chlorophyll-a and chlorophyll-b pigments in photosystem I (PSI) and photosystem II (PSII) [28]. Previous studies have applied HCFM and MCR analysis to visualize differential localization and relative quantification of chlorophyll pigments in the two photosystems in cyanobacteria, algae, and plants [29-32]. The ability of HCFM to detect changes in photosynthetic pigment abundance and localization at the individual cell level makes this technique well-suited to visualize spatial changes in plant pigments resulting from metal stress.

Tall fescue (*Festuca arundinacea*) is a perennial grass found throughout the world. It is one of the most plentiful grasses in the United States, covering over 35 million acres and serving important purposes, such as pasture feedstock and soil erosion prevention [33]. Tall fescue has been extensively studied for its abilities in phytoremediation due to its high tolerance of heavy metals and its easy cultivation [34]. Prior literature has shown phytoremediation potential of tall fescue in heavy metals including cadmium (Cd), lead (Pb), and zinc (Zn), with Cd being the most promising [35-37]. Cadmium (Cd) tolerance in tall fescue has been attributed to preferential Cd accumulation in mature leaves relative to emerging leaves and its ability to excrete Cd through the leaf cuticle layer [38, 39]. While tall fescue has shown promise for phytoremediation of Cd, studies with Cr(VI) have shown low Cr(VI) uptake and increased stress responses, including reduced chlorophyll and decreased photosystem II (PSII) activity [40-42]. Tall fescue has also shown low tolerance to Cu stress, with reduced biomass and chlorosis at Cu concentrations above 50 mg/kg soil [43]. While these studies have shown that Cr(VI) and Cu are toxic to tall fescue, microscopic spectral analysis is needed to understand the changes in cellular structure and pigment localization that contribute to these macroscopic phenotypes.

This study examines the toxic effects of Cr(VI) and Cu exposure in tall fescue to further understand its stress responses at the microscopic level. Acute Cr(VI), Cu, and varying levels of combined Cr(VI)/Cu stresses were applied to tall fescue, and for nine days following treatment, measurements were collected to assess bulk phenotypic changes and corresponding microscopic changes using standard brightfield and confocal fluorescence microscopy and HCFM with MCR analysis. We also conducted an experiment of chronic Cr(VI) exposure to simulate more realistic environmental conditions, as previously reported groundwater concentrations of Cr(VI) contamination are significantly lower than the acute Cr(VI) dose. In the chronic Cr(VI) experiment, we applied two doses of Cr(VI) to tall fescue daily over the course of 27 days. The low dose was calculated based on the concentration of Cr measured in water collected from the Hanford site in 2008 [44], and the high dose was calculated based on the amount needed to achieve accumulation of 250 mg of Cr(VI) in 11 days, the minimum amount required to produce a visible stress response in tall fescue (data not shown). The same bulk and microscopic measurements were taken to assess the chronic stress response of tall fescue. These results provide insight into the structural and global pigment changes associated with acute and chronic metal stress responses in tall fescue. Additionally, we identify a new fluorescence feature associated with the formation of microscopic globular bodies in tall fescue in response to metal stress.

2. Materials and Methods

2.1 Materials

Festuca arundinacea Shreb. (tall fescue) seeds from Barolex cultivar were kindly provided by Dr. Michelle DaCosta at the University of Massachusetts, Amherst; these were originally purchased from Albert Lea Seed (Albert Lea, Minnesota). Soil, Premier Horticulture 20380RG PRO-Mix HP High Porosity Grower Mix, was purchased from Esbenshades Garden Center (Lititz, Pennsylvania). Topsoil, Premier Horticulture Pro PGX Loose Plug and Germination Mix,6 inch planter nursery pots, 6 inch clear saucers (Hydrofarm HGS6), grow trays (20” × 10”), and a 6-inch vented plastic dome (20” × 10”, Planters Pride RZD102H) were procured from Amazon. Miracle-Gro water soluble all-purpose plant food was purchased from Walmart. Chemicals (5% potassium chromate, potassium chloride, and copper(II) chloride dihydrate) were obtained from Fisher Scientific.

All plants in this experiment were cultivated in the laboratory using *Festuca arundinacea Shreb.* (tall fescue) seeds provided by our collaborator, Dr. Michelle DaCosta. These seeds were originally purchased from Albert Lea Seed (Albert Lea, Minnesota). Tall fescue is not endangered, and therefore, is not subject to additional regulation. All research was conducted in accordance with our institutional ethics policy and approved by an institutional biosafety committee.

2.2 Growth and Stress Treatment

Tall fescue was seeded at 15 mg per square inch in 6-inch planters containing PRO-Mix HP High Porosity Grower Mix (Premier Horticulture, Inc., containing 75% sphagnum peat moss and 25% perlite) saturated with deionized water and 150 mL of Miracle-Gro water soluble all-purpose plant food. Seeds were covered with topsoil (Premier Horticulture Pro PGX Loose Plug and Germination Mix) and hydrated by misting deionized water from a spray bottle. Seeded planters were placed in 6-inch plastic saucers, arranged on grow trays, covered with a vented plastic dome to retain

moisture, and placed in a photosynthetic incubator (Shellab, Model LI15-ZZMFG) at 25°C with solar LED lights from BuildMyLED at a light intensity of 150-200 µmol photons m^{-2} s^{-1} and a 16:8 light:dark cycle. The planters were misted with deionized water daily until seedlings sprouted. After the seedlings reached the height of the plastic dome, the dome was removed. Deionized water was added to the saucer to maintain moist soil (either daily or every other day), and 150 mL of Miracle-Gro was added to the saucer once a week.

After seven weeks of growth, tall fescue was exposed to the metal stress conditions. Tall fescue planters were not watered for two days prior to the addition of the metal solutions to facilitate rapid uptake. Two stress treatments were analyzed in this study: (1) acute Cu and Cr(VI) stress and (2) chronic Cr(VI) stress. The acute stress experiment included eight planters and six different treatments: an untreated control, Cu only (1000 mg Cu per kg soil), Cr(VI) only (500 mg/kg Cr(VI) per kg soil), two replicates of severe co-stress (250 mg Cr(VI) per kg soil and 500 mg Cu per kg soil), two replicates of moderate co-stress (200 mg Cr(VI) per kg soil and 400 mg Cu per kg soil), and one replicate of light stress (150 mg Cr(VI) per kg soil and 300 mg Cu per kg soil). Cr(VI) was provided from a 5% solution of potassium chromate (K_2CrO_4), and Cu was delivered through a 0.2 M solution of $CuCl_2$. A total of 100 mL of each metal solution was delivered to each planter, using a 0.515 M solution of potassium chloride to provide an equivalent level of potassium and chloride ions to all planters. Treatments were applied after acquiring all day 0 measurements. The chronic stress experiment included six planters and three treatments: two untreated control replicates (water added daily to maintain soil moisture), two low dose replicates (75 µg of Cr(VI) per day), and two high dose replicates (22.5 mg of Cr(VI) per day). The amount of water added to planters was variable and based on the amount needed to keep the soil moist but not oversaturated.

2.3 Photosynthetic Yield Measurements and Digital Images

Leaf blades, visually representative of the overall plant, were bundled together and covered with a leaf clip to shield the leaves from light for dark adaptation. Two leaf clips were used on each planter. After 30 minutes of dark adaptation, pulse amplitude modulated (PAM) fluorescent measurements were taken from the blades within the leaf clip using a photosynthesis yield analyzer (Walz, MINI-PAM-I). The PAM gain and measurement interval were set to 3 and 1 respectively with burst mode turned off to prevent measurement saturation. A black background was used to blank the auto-zero prior to measurement acquisition. Photosynthetic yield measurements were acquired on days 0, 1, 2, 3, 4, 7, and 9 for the acute stress experiment and on days -1, 9, 13, 16, 20, 23, and 27 for the chronic stress experiment. Digital images of the tall fescue planters were taken the same days as the photosynthetic yield measurements to visually qualify physical changes using a Canon Rebel T2i DSLR camera.

2.4 Preparation for Microscopy

Young leaf blades were selected from the central portion of the blade sheaths surrounding the crown/shoot (leaves that split from the main blade stem). Two leaf blades, visibly representative of the overall plant condition, were removed from each planter and cross-sectioned for both confocal fluorescence microscopy and hyperspectral confocal fluorescence microscopy measurements using a precision double edge razor blade (Personna, Inc.). Leaf sections were cut into thin strips and placed on their lateral side to expose the cross-sectional area of the leaf with the assistance of a

dissection microscope. The cross-sections were placed on #1.5 24 × 60 mm cover slips (Corning, Cat No. 2980-246) for brightfield and confocal fluorescence imaging and on a 25 × 75 × 1 mm glass microscope slide (Fisher Scientific, Cat No. 12-544-2) for HCFM. Supplemental water was placed on and around leaf sections on the coverslips to ensure sufficient hydration during microscopy and assist with adhesion of the cross-section to the cover slip. Cross-section images were taken for each blade, with particular emphasis on the center nodes. Dehydrated sections resulted in anomalous results due to shriveled tissue and were not imaged.

2.5 Confocal Brightfield and Fluorescence Microscopy

Multiple cross-sections from each dissected leaf blade were imaged using a Leica DMi8 DLS confocal fluorescence microscope equipped with a Leica HC PL APO CS2 20x/0.75 objective (Leica Microsystems, Model #11506517). LAS X Version 3.5.2.18963 by Leica Microsystems ©2018 was used as the image acquisition software. Three laser diode excitation sources were used (488 nm, 552 nm, and 638 nm) at a 0.5% power setting with a Leica SP8 LIAchroic low incident angle dichroic beam splitter. Imaging was completed on a Leica SP detector scan head with photomultiplier tube (PMT) detectors. Chlorophyll fluorescence was detected using a 660-690 nm spectral window with a PMT gain of 500. Transmitted light was collected using a PMT gain of 225-250. All images were collected using sequential scanning between frames with a resonance scanner at a speed of 8,000 Hz (28 fps at 512*512 pixels) at a zoom of 1.25x. Line averaging of 4 was used to improve signal-to-noise. All images were collected as a 75.37 µm 111-slice z-stack with an axial step size of 0.69 µm at an X*Y image size of 125 µm*125 µm and a pixel size of 244.62 nm*244.62 nm. A total of 5-8 images were collected per leaf blade.

2.6 Quantification of Confocal Chlorophyll Fluorescence

To assess chlorophyll fluorescence from the confocal fluorescence images taken from each cross-section, custom software developed in MATLAB (Mathworks, Natick, MA, USA, version R2020b) was utilized in combination with Image J (Fiji) 1.52p [45]. A Matlab function was developed to identify the set of 10 frames within the confocal Z stack that was most in focus. The first step of the process was to differentiate pixels which had signal (chlorophyll fluorescence) from noise pixels. This was achieved by calculating the maximum intensity z-projection and calculating the average and standard deviation using a robust, median-based estimate of the standard deviation [46]. The threshold differentiating signal from noise pixels in the maximum intensity z-projection was then set to the estimated average value plus six times estimated standard deviation. For pixels containing fluorescence, the fluorescence intensity was maximized when those fluorophores were most in focus, maximizing the ensquared energy of the point spread function. Therefore, for all signal pixels, the indices of the 10% of brightest frames were computed, and the distribution (histogram) of these indices was computed across the entire image with maximum of the histogram defining the best average focus. Automated frame selection was verified by visual examination from a trained user. Image J (Fiji) 1.52p was then utilized to create a 10-slice image projection from the center slice determined above (Image → Stacks → Z Project → Average Intensity). A threshold was applied to segment out the chlorophyll pigment (Image → Adjust → Threshold → 15-255, Isotype, Red, √ Dark Background → Apply). The resulting image was then analyzed for three statistical measurements including chlorophyll fluorescence intensity and overall fluorescence area measurements (Analyze

→ Set Measurements → Area, Area Fraction, and Mean Gray Value). For average intensity measurements, the pixels that did not contain any signal were processed as 'NaN' in Image J to not affect the overall chlorophyll fluorescence mean intensity. Cross-sectional area measurements determined from the brightfield images (Supplemental file, Methods and Figure S3) were used in conjunction with chlorophyll fluorescence measurements to determine the % area of the plant containing chlorophyll; the chlorophyll area, determined by Image J (Fiji) 1.52p, was divided by the leaf section's cross-sectional area and multiplied by 100%. The mean intensity and % area containing chlorophyll were then graphed in GraphPad Prism© 2020, and statistical quantification was determined through a Kruskal-Wallis statistical test.

2.7 Hyperspectral Confocal Fluorescence Microscopy

Dissected cross-sectional leaf blades, as described above, were imaged using a custom hyperspectral confocal fluorescence microscopy system which has been detailed previously [27]. The general imaging methodology has been described previously for assessing chlorophyll pigments in living cells [28, 47]. In brief, we utilized a 488 nm laser light that was focused through a 10x objective (Nikon Plan Apochromat; numerical aperture 0.45) to a diffraction-limited spot. Fluorescence was collected through the same objective, dispersed by a custom-made prism spectrometer, and detected by an electron-multiplied CCD array (Andor Technologies) [27]. At least 8-10 images were collected per leaf, totaling ~20 images per planter.

2.8 Analysis of Hyperspectral Confocal Fluorescence Microscopy Data

Preprocessing and MCR analysis was performed on a composite data set consisting of a representative set of hyperspectral confocal fluorescence images from all the conditions and timepoints in the acute exposure experiment as previously described [48]. In-house written MCR software [49] executed in Matlab (Mathworks, Natick, MA, USA, version R2020b) was utilized to develop a 4 component spectral model that describes >95% of the variance from the hyperspectral confocal fluorescence images of the plant tissue. Spectral residuals were inspected to confirm the goodness of fit of the model and consisted primarily of random noise. The MCR-identified spectral model was utilized to predict the relative concentration and location of each spectral component in all of the images from the acute and chronic data sets via a classical least squares prediction algorithm. Spectral residuals were inspected to confirm the goodness of fit of the model to the chronic exposure data set and similar to the acute exposure data set, consisted primarily of random noise.

Standard image processing was employed on each of the resulting concentration maps to obtain quantitative statistics of the three chlorophyll spectral features in the dissected leaf sections. Image J (Fiji) 1.52p was utilized for thresholding and quantification. A custom written macro was created to process the RGB composite images based on a specified threshold value for each spectral channel to then calculate the overall image statistics. The following thresholds were applied to each of the concentration maps: Chl-a: 500-Max, Chl-b: 500-Max, PSI: 400-Max, and Broad AF: 50-Max. The resulting image was then analyzed for 10 statistical measurements including chlorophyll fluorescence intensity and overall fluorescence area per image (Analyze → Set Measurements → Area, Standard Deviation, Min and Max Gray Value, Integrated Density, Area Fraction, Mean Gray Value, Perimeter, Fit Ellipse, Feret's diameter, Median). The measurements from the same planters

and conditions were averaged together to compare different stress treatments. Data were graphed in GraphPad Prism© 2020 Ver. 9.1.1, and statistical quantification was determined through a Kruskal-Wallis statistical test.

Additional measurements were made to quantify the intensity, size, and number of globular bodies in the HCFM images from the acutely stressed plants that exhibited this stress response (moderate co-stress days 7 and 9; severe so-stress days 4, 7, and 9) and the chronic Cr(VI) stressed plants (days 15, 22, and 29). Custom Matlab routines (Mathworks, Natick, MA, USA, version R2020b) performed segmentation of the globular bodies from the MCR generated concentration maps corresponding to the globular bodies. Segmentation was accomplished by manual identification of boundaries. Once segmentation was complete, the number of bodies was calculated per image along with the area of each body and the mean fluorescence emission intensity from each body. Data were graphed in GraphPad Prism© 2020 Ver. 9.1.1, and statistical quantification was determined through a Kruskal-Wallis statistical test.

3. Results

3.1 Acute and Chronic Metal Treatments Lead to Visible Stress and Reduced Photosynthetic Yield in Tall Fescue

To study metal stress response in tall fescue, we applied both acute and chronic stress treatments. Digital pictures were taken to visually assess changes in phenotype, and photosynthetic yield measurements provided a quantitative assessment of plant health.

The acute stress experiment included six treatments: untreated control, Cu (1000 mg Cu per kg soil), Cr(VI) (500 mg/kg Cr(VI) per kg soil), light co-stress (150 mg Cr(VI) per kg soil and 300 mg Cu per kg soil), moderate co-stress (200 mg Cr(VI) per kg soil and 400 mg Cu per kg soil), and severe co-stress (250 mg Cr(VI) per kg soil and 500 mg Cu per kg soil). For acute stress, the metal treatment was applied on day 0, and water was added daily to maintain soil moisture. Visible signs of stress were observed the first day after treatment for the Cu, Cr(VI), and severe co-stress treatments (Supplemental file, Figure S1). At nine days post-exposure to acute metal stress, tall fescue displayed observable changes to leaf coloring and physical appearance under all stress treatments (Figure 1A). The untreated control plant grew during the 9-day study, maintaining an overall healthy phenotype with only a few necrotic leaves in the planter. Cu and Cr(VI) treatments exhibited significant stress responses to the metals including necrosis (browning), chlorosis (yellowing), loss of turgor, and reduction in leaf size. The Cu treatment had more necrosis while the Cr(VI) treatment had more chlorosis. The light co-stressed fescue exhibited minimal chlorosis and losses in leaf turgor, along with small amounts of shriveling. The severity of this stress phenotype was dose dependent, as the effects were exaggerated in the moderate co-stressed fescue and even more so in the severe co-stressed fescue. All metal treated tall fescue shoots exhibited heterogeneity in stress responses throughout the planter, potentially indicating variable rates of leaf uptake or stress response based on the location of the roots within the planter relative to dispersion of the metals in the soil or due to the age of the plant or leaf. Photosynthetic yield measurements support the observed changes in visible phenotype (Figure 1B). The untreated control planter had little to no change in photosynthetic yield during the nine days following treatment. Photosynthetic yield for both the Cu and Cr(VI) treated plants decreased following treatment until day four, after which each showed some recovery. This recovery is likely due to the few healthy leaf blades that survived in each planter.

The light co-stressed tall fescue showed little to no changes, except for a slight, but noticeable decrease on day 3, before recovering. By day 2, moderate co-stressed fescue plants had significantly decreased photosynthetic yield. This decrease did not continue, nor did the plants recover. This effect was exaggerated in the severe co-stress treatment, showing a dose dependence between light, moderate, and severe co-stress treatments.

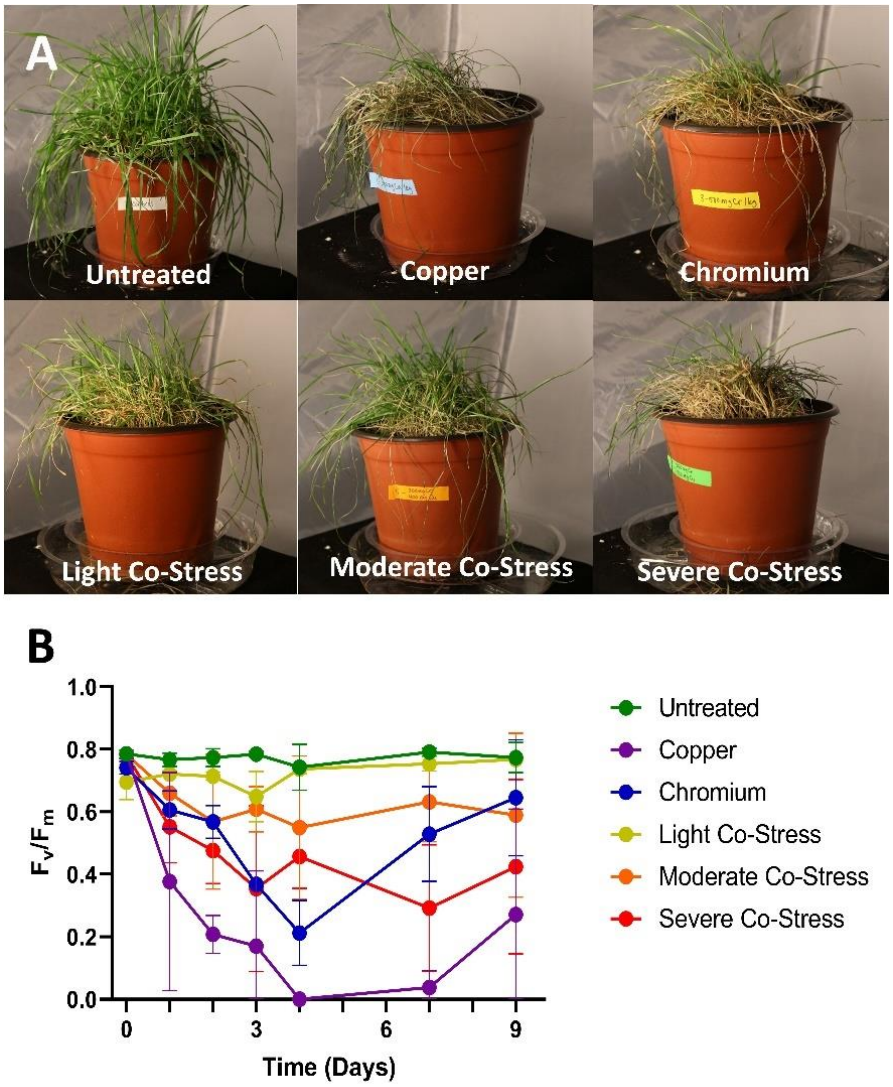

Figure 1 Physiological characterization of tall fescue after acute metal stress treatment. (A) Digital images on day 9 and (B) photosynthetic yield measurements across the time course of the experiment. Photosynthetic yield measurements are averages of two dark-adapted measurements taken from different leaves in the treated planter with error bars indicating the standard deviation.

For the chronic stress experiment, treatments were applied daily for a total of 27 days and consisted of untreated controls (water only), low Cr(VI) dose (75 µg of Cr(VI) per day), and high Cr(VI) dose (22.5 mg of Cr(VI) per day). Similar to the acute stress experiment, the untreated controls showed increased biomass and generally maintained a visually healthy phenotype with some necrotic leaves in each planter (Figure 2A and Supplemental file, Figure S2). The low chronic Cr(VI) dose did not elicit any physical or visual changes relative to the untreated controls. The high Cr(VI)

dose resulted in chlorosis and necrosis of leaves, losses in rigidity and turgor, and shriveling. Within a single planter, the tall fescue plant shoots displayed heterogeneity in stress response under the high Cr(VI) dose, with some shoots maintaining a healthy phenotype even after 27 days of Cr(VI) application (Figure 2A). Photosynthetic yield measurements correlated with visible phenotypes in the chronic stress experiment (Figure 2B). Only the high Cr(VI) dose resulted in significant changes in photosynthetic yield. The decrease in photosynthetic yield for the high chronic dose condition was delayed relative to the acute stress experiment (Figure 2B vs Figure 1B), with significant decline after day 14. On day 14, the fescue planters had been exposed to a cumulative dose of 0.315 g of Cr(VI) (22.5 mg/day × 14 days), which is close to the minimum acute Cr(VI) treatment leading to a visible stress phenotype (0.250 g, data not shown).

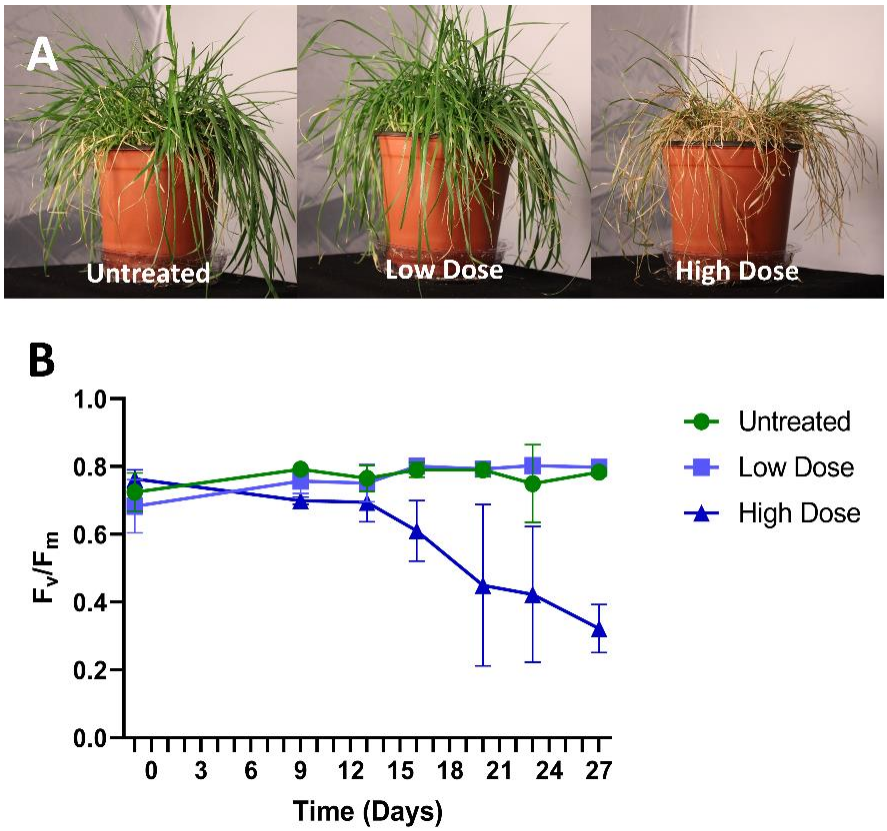

Figure 2 Physiological characterization of tall fescue after chronic Cr(VI) stress treatment. (A) Digital images on day 27 and (B) photosynthetic yield measurements across the time course of the experiment. Photosynthetic yield measurements are averages of two dark-adapted measurements taken from different leaves in the treated planter with error bars indicating the standard deviation.

3.2 Acute Copper and Chromium Stress Alters the Localization and Concentration of Photosynthetic Pigments in Tall Fescue

To quantify structural and pigment changes in tall fescue in response to acute Cu, Cr(VI), and co-stress conditions, we performed brightfield and confocal chlorophyll fluorescence imaging to assess structural changes within the plant tissue and average chlorophyll fluorescence levels. Simultaneously, HCFM was also conducted on the same plants each day to provide spectrally-

resolved fluorescence emission data. MCR analysis allowed spectral separation of the different chlorophyll pigments [Chl-a, Chl-b, and Chl associated with photosystem I (PSI)] and prediction of their relative abundances within the plant tissue. HCFM also permitted identification of an additional spectral feature indicative of the stress response.

Over 80 brightfield and chlorophyll fluorescence images were collected from two leaves from tall fescue planters treated with each condition. Representative brightfield and chlorophyll fluorescence images for each treatment are shown in Figure 3A. Visualization of the untreated tall fescue leaves revealed that chlorophyll (Figure 3A, red) is localized within the chloroplasts in the sides of the leaf cross-sections, away from the main vascular bundles. The overall chlorophyll signal is reduced with metal stress, especially in the Cu, Cr(VI), and severe co-stress treatments. Quantification of the chlorophyll fluorescence intensity and chlorophyll area nine days after acute stress treatment is shown in Figure 3B and Figure 3C. Chlorophyll area and chlorophyll fluorescence intensity for light co-stressed tall fescue was not statistically reduced compared to the untreated control. Essentially no chlorophyll fluorescence was observed in Cu treated fescue plants at day 9. The Cr(VI), moderate co-stress, and severe co-stress exposed fescue all had significantly reduced chlorophyll fluorescence intensity and average chlorophyll percent area as compared to untreated control.

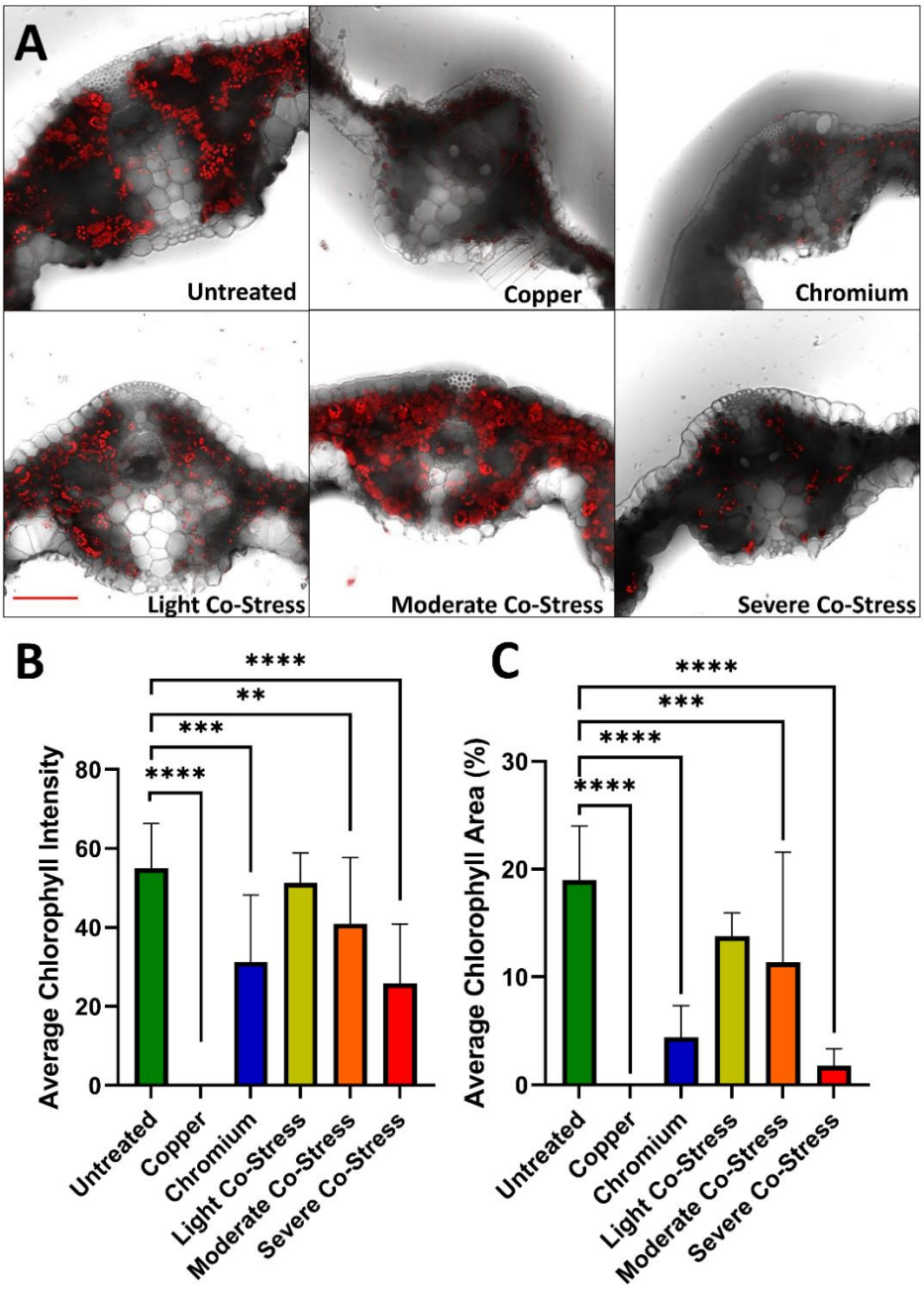

Figure 3 Brightfield and confocal fluorescence microscopy along with chlorophyll quantitation from tall fescue exposed to acute metal stress. (A) Brightfield images overlaid with confocal chlorophyll fluorescence images (red) of tall fescue cross-sections nine days after acute metal stress treatment. The red scale bar is 100 µm. (B) Average chlorophyll intensity and (C) average percentage of leaf area containing chlorophyll normalized to the leaf area from confocal chlorophyll fluorescence images. * Designates statistical significance: * $p < 0.05$, ** $p < 0.01$, *** $p < 0.001$, **** $p < 0.0001$.

In addition to quantifying chlorophyll, we analyzed the following structural features within the tall fescue tissue: area of the vascular bundle fiber, area of the abaxial fiber bundle, area of the adaxial fiber bundle, and area of the metaxylem elements, along with three measurement references for normalization: area of the leaf cross-section, vertical length of the cross-section, and vertical length of the cross-section sides (Supplemental file, Figure S3). The average values for each

structural feature normalized to the area of the leaf cross-section for all acute treatments over the experimental time course are shown in Figure S4 (Supplemental file). Overall, we observed dramatic structural changes, such as shriveled tissue and distorted cross-sections for the Cu, Cr(VI), and severe co-stress treatments nine days after acute exposure. However, quantification of the structural features did not show any statistically significant changes due to high variability between shoots in each treated planter.

HCFM was performed on cross-sections of tall fescue leaves similar to the brightfield and fluorescence confocal measurements described above (2 leaves from each plant, multiple areas imaged per leaf). An MCR-generated mathematical model containing four overlapping chlorophyll spectra was found to accurately represent the pigment contributions from a composite set containing data across all conditions on all days (Figure 4). These spectra represent the distinct chlorophyll species contributions under the primary chlorophyll peak and arise from Chl-a, Chl-b, PSI, and a newly identified broad spectrum feature we termed broad autofluorescence (broad AF). The spatial distribution of each of the chlorophyll spectral components are shown in Figure 5A for representative images from each condition on days 0, 4, 7 and 9, respectively (see Figure S5 in Supplemental file for an illustration of how the individual pigment images are merged into the composite images shown in Figure 5A). On day 4, changes in pigment relative abundance and localization are evident for the three co-stress treatments going from little to no change in cellular structure at the low co-stress to subtle but clear clumping. The moderate and severe co-stress treatments show a distinct loss of Chl-a at the moderate and severe co-stress treatment and an appearance of the broad AF emission component (white circular features) at the highest co-stress treatment. The Cu and Cr(VI) treatments show a loss of structure/chloroplast boundaries and pigment changes with an increase in PSI (blue) as compared to the untreated control. This trend continues to increase in severity over time, and the day 9 images show additional reduction in pigment abundance, particularly for Chl-a along with degradation of the chloroplast boundaries. In the severe co-stress condition, a distinct clumping is seen, and this is accompanied by the development of the autofluorescent globular bodies. We note that although the images in Figure 5A are considered representative, there was a high degree of planter-to-planter variability as well as leaf-to-leaf variability within a planter.

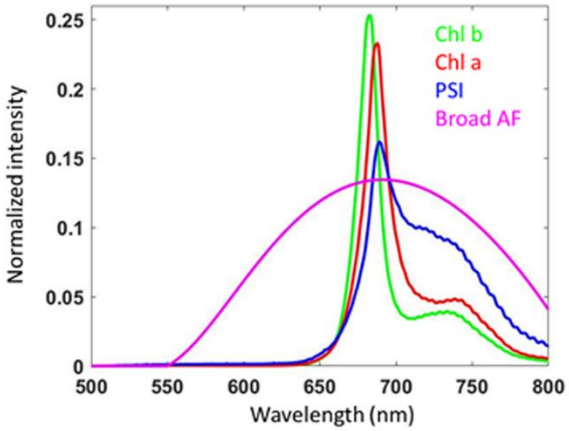

Figure 4 MCR identified component emission spectra from HCFM images of metal stressed tall fescue. Traces are normalized to unit length.

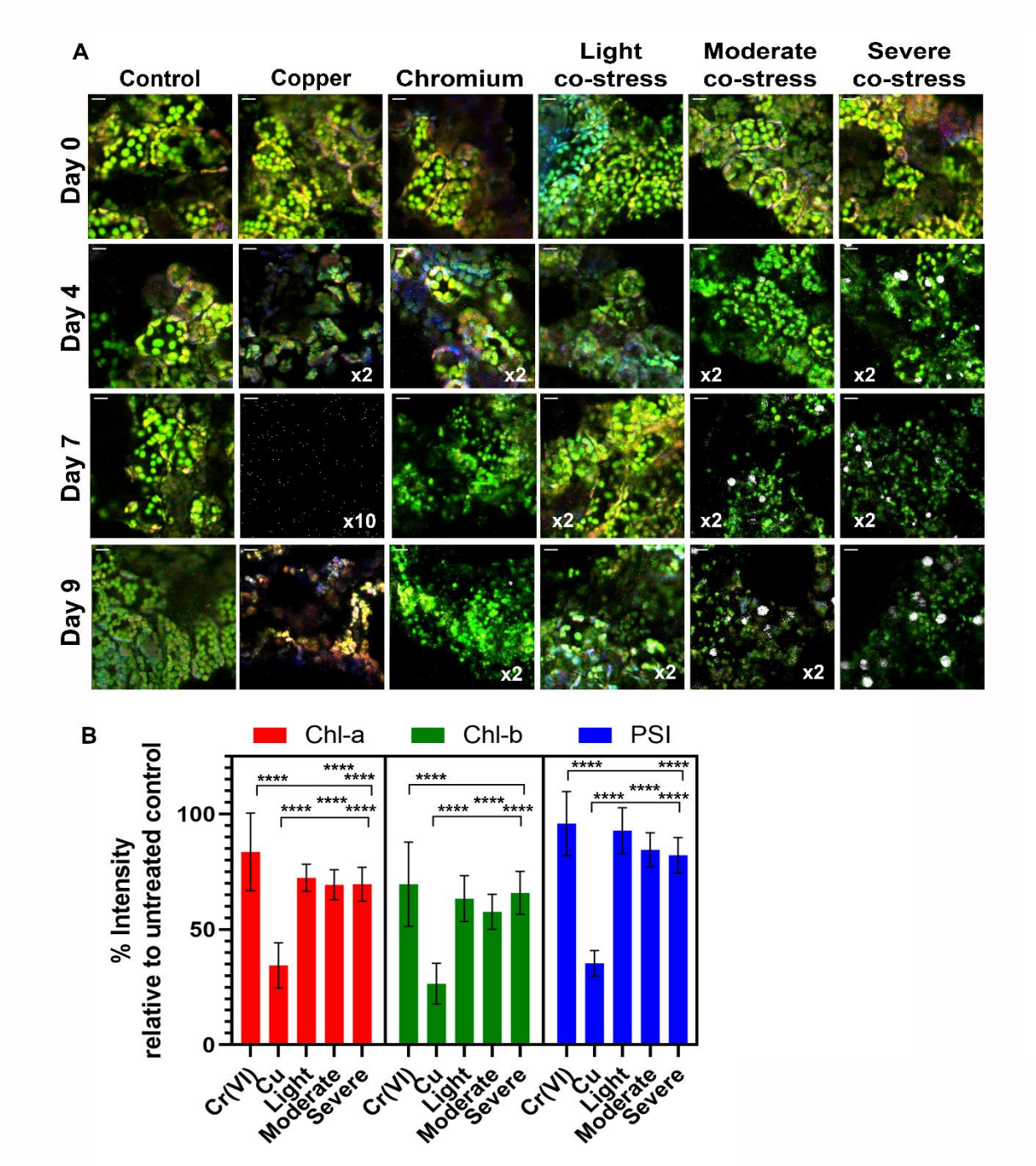

Figure 5 A. Representative images from MCR analysis of HCFM images of tall fescue leaf cross-sections following acute metal stress treatment. The colors in composite image correspond to the spectral component colors in Figure 4, with the exception of the broad AF feature: Chl-a = red, Chl-b = green, PS1 = blue, broad AF = white. Unless otherwise noted, color intensities are plotted on the same relative color scale making the images visually comparable. The x2 and x10 notations indicate the abundances in that image have been multiplied by 2 or 10, respectively, to make the features visible. The scale bar is equal to 10 µm. B. Quantification of relative abundances of the photosynthetic pigments Chl-a (left plot, red), Chl-b (middle plot, green), and PSI (right plot, blue) on Day9. **** Designates statistical significance, $p < 0.0001$.

Using the processed HCFM data, we quantified the relative abundance of Chl-a, Chl-b, and PSI in each spectral component. Day 9 is shown in Figure 5B, while quantification over all days and all conditions is shown in Figure S7 (Supplemental file). The Cu treatment had the strongest reduction in pigment signal, losing ~70% of the Chl-a and Chl-b emission and ~60% of the PSI relative to the untreated controls. In all three co-stress treatments (light, moderate, and severe), Chl-a and Chl-b decreased more significantly than PSI.

Further analysis of the broad AF feature was conducted to evaluate if the globular bodies associated with it were growing in fluorescence intensity, area, or both. We evaluated the number of bodies, mean fluorescence intensity of the bodies, and area of the globular bodies (Figure 6). While there was no consistent trend in the number of globular bodies across time, the number of bodies was much higher under the severe co-stress condition relative to the moderate co-stress condition for all days (Figure 6A). Similarly, the mean fluorescence intensity of the broad AF feature was also higher for the severe co-stress condition compared to the moderate co-stress treatment, with no major temporal trend (Figure 6B). The area of the broad AF feature was only higher for the severe co-stress treatment at day 9 compared to the moderate co-stress condition, and an increasing temporal trend in area was observed under the severe co-stress treatment (Figure 6C).

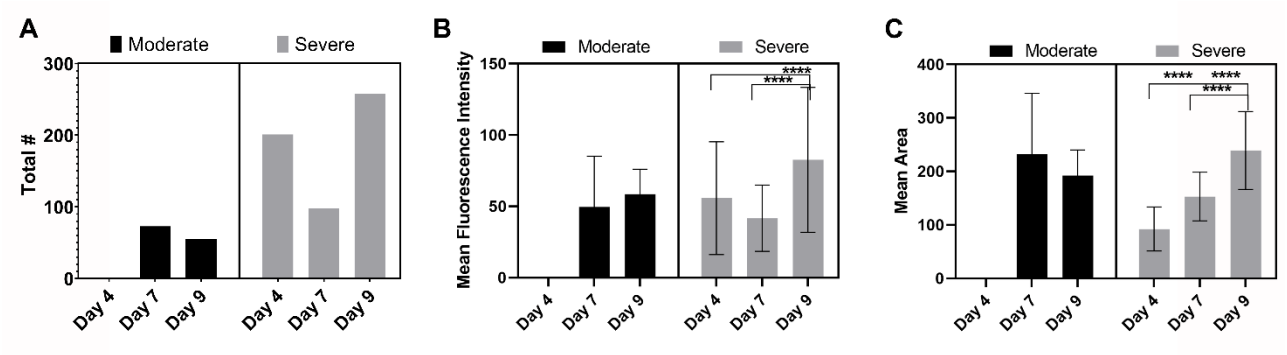

Figure 6 Characterization of globular bodies observed under acute metal stress treatment of tall fescue. A: Total number of globular bodies. B: Mean fluorescence intensity of individual globular bodies. C: Mean area of individual globular bodies. * indicates statistical significance, **** $p < 0.0001$.

3.3 Chronic Chromium Stress Alters the Localization and Concentration of Photosynthetic Pigments in Tall Fescue

For the chronic Cr(IV) stress experiment, confocal fluorescence microscopy and HCFM were conducted on tall fescue, as described in 3.2 for the acute stress experiment. Confocal fluorescence microscopy of untreated tall fescue again revealed that chlorophyll (Figure 7, red) was localized in the sides of the leaf cross-sections, outside of the main vascular bundles. Chlorophyll abundance was visibly reduced for the high chronic dose of Cr(VI), but no visible changes in chlorophyll were readily apparent for the low chronic Cr(VI) dose. Statistical analysis of mean chlorophyll fluorescence intensity and percent area are shown for each treatment on day 27 in Figure 7B and Figure 7C. Quantification of chlorophyll from tall fescue stressed from chronic Cr(VI) exposure revealed that the low Cr(VI) dose reduced chlorophyll fluorescence intensity, although this was not readily apparent from visual inspection of the images. However, only the high Cr(VI) dose reduced the area of chlorophyll within the leaf cross-section. The reduction in percent area containing

chlorophyll for the high Cr(VI) dose treatment was much larger than the reduction in its chlorophyll fluorescence intensity. As previously described in the acute metal stress experiment, structural changes were also measured (Supplemental file, Figure S6). Similar to the acute stress experiment, changes in these structural features were not statistically significant due to the high variability between leaf cross-sections.

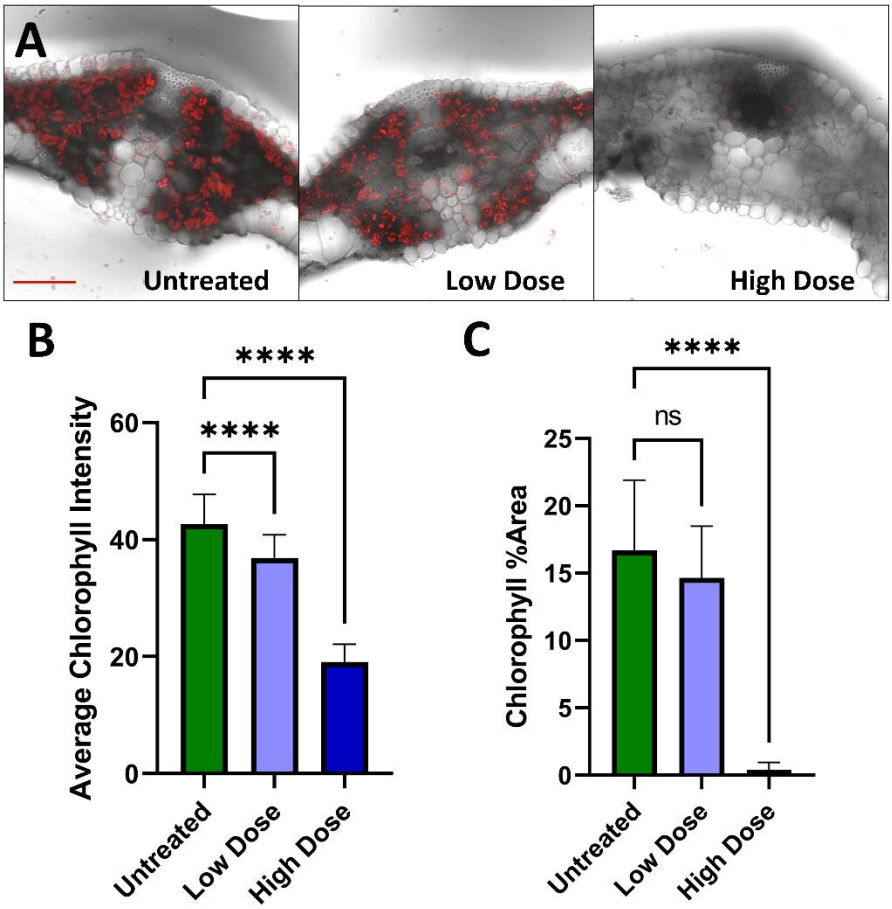

Figure 7 Brightfield and confocal fluorescence microscopy along with chlorophyll quantitation from tall fescue exposed to chronic Cr(VI) stress. (A) Brightfield images overlaid with confocal chlorophyll fluorescence images (red) of tall fescue cross-sections 27 days after acute metal stress treatment. The red scale bar is 100 µm. (B) Average chlorophyll intensity and (C) average percentage of leaf area containing chlorophyll normalized to the leaf area from confocal chlorophyll fluorescence images. * Designates statistical significance, **** $p < 0.0001$.

HCFM was also performed on cross-sections of tall fescue leaves during the chronic Cr(VI) experiment. HCFM data was collected on days 2, 9, 15, 22, and 29. The same model containing three overlapping chlorophyll spectra and a broad autofluorescence feature that was developed for the acute stress treatment image data was also found to accurately represent the pigment contributions from a composite set containing data from the chronic stress treatment across all conditions on all days (Figure 4). Representative images from each condition at days 2, 9, 15, 22, and 29 are displayed in Figure 8A. The low Cr(VI) dose displayed small to subtle changes in pigment localization and pigment abundances as compared to the untreated control plants. The high Cr(VI) dose showed a

loss of chloroplast structure and pigment changes with relatively large decreases in Chl-a, Chl-b, and PSI pigments and appearance of globular bodies starting at day 15 (Figure 8A). Quantification of the fluorescence spectra for each pigment confirmed decreased pigment content for the high dose treatment, with Chl-a and Chl-b showing greater reduction compared to PSI (Figure 8B). Quantification of photosynthetic pigments across all days of the chronic experiment is shown in Figure S8 (Supplemental file). The broad AF feature was again characterized by quantifying the number of globular bodies, mean fluorescence intensity, and mean area (Figure 9). The number of globular bodies and the mean fluorescence intensity of the broad AF feature dramatically increased over time while the mean area of the globular bodies increased between days 15 and 22 but decreased by day 29.

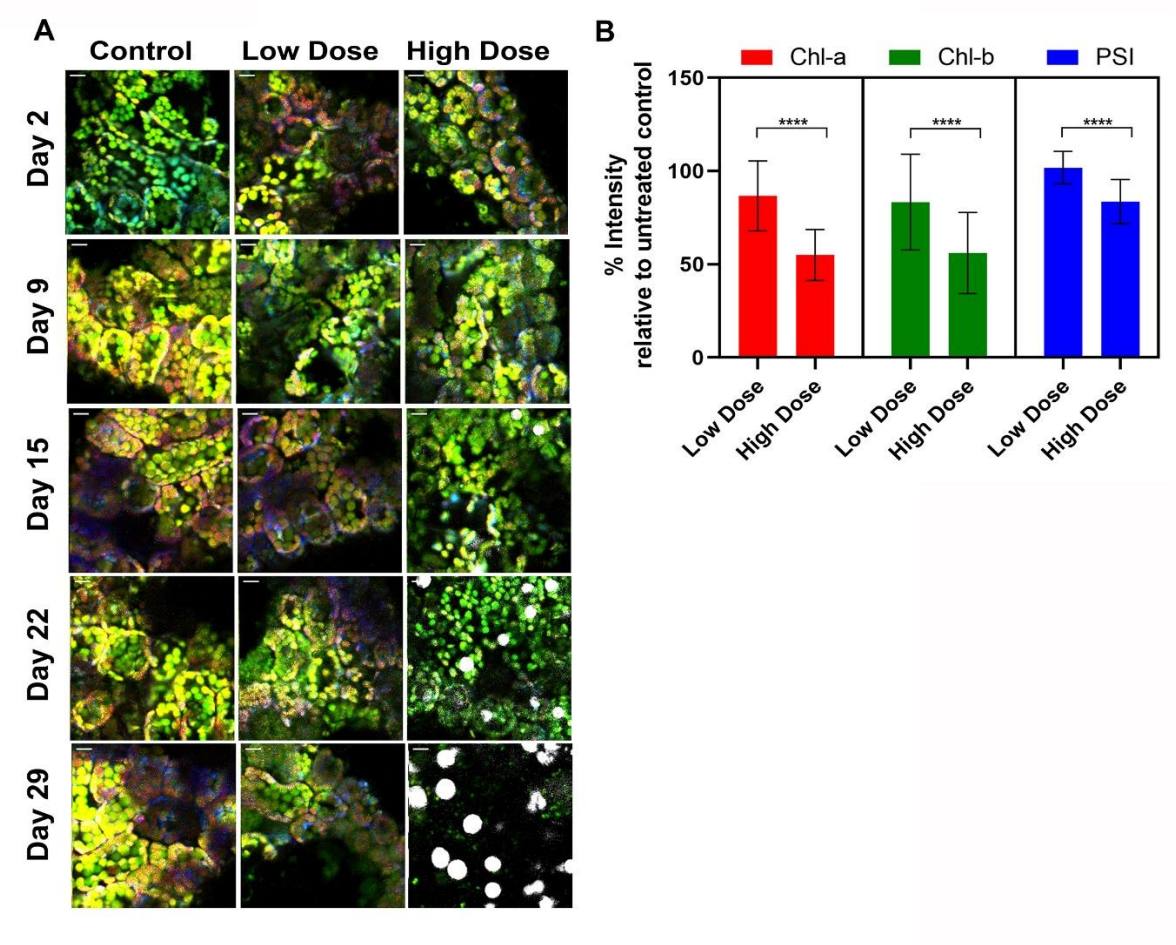

Figure 8 A. Representative images from MCR analysis of HCFM images of tall fescue leaf cross-sections following chronic Cr(VI) treatment. The colors in composite image correspond to the spectral component colors in Figure 4: Chl-a = red, Chl-b = green, PS1 = blue, broad AF = white. All color intensities are plotted on the same relative color scale making the images visually comparable. The scale bar is equal to 10 µm. B. Quantification of relative abundances of the photosynthetic pigments Chl-a, Chl-b, and PSI on Day 29. * Designates statistical significance, **** $p < 0.0001$.

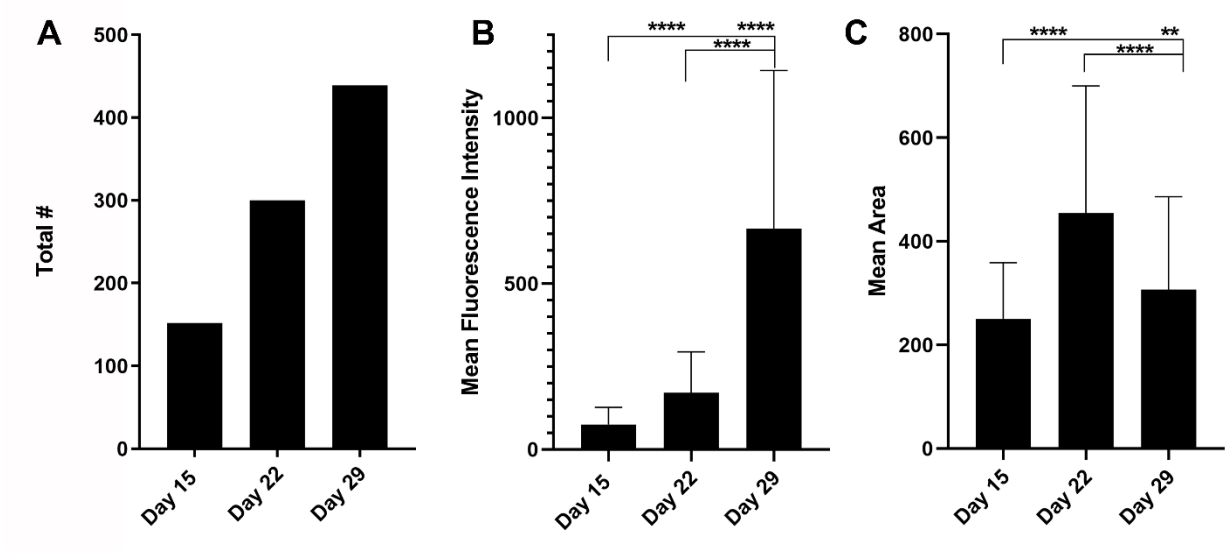

Figure 9 Characterization of globular bodies observed under chronic metal stress treatment of tall fescue. A: Total number of globular bodies. B: Mean fluorescence intensity of individual globular bodies. C: Mean area of individual globular bodies. * indicates statistical significance, ** $p < 0.01$, **** $p < 0.0001$.

4. Discussion

While tall fescue has shown promise for bioremediation of some metal contaminants in the environment, both Cr(VI) and Cu have been shown to cause stress [43, 50-52]. In this study, we evaluated the effect of both acute and chronic metal stress on tall fescue using bulk phenotypic characterization along with microscopy to assess pigment concentration and localization at the cellular level. For the acute stress experiments, Cr(VI) stressed plants showed visible signs of chlorosis (i.e., yellowing), while Cu stress resulted in a necrotic phenotype (i.e., browning) (Figure 1A). Thus, while both Cr(VI) and Cu are believed to cause stress through accumulation of ROS [53, 54], these phenotypes indicate that there may be some difference in the mechanism of plant stress. Conventional confocal fluorescence microscopy and hyperspectral confocal fluorescence microscopy provided further insight into changes in photosynthetic pigments associated with metal stress in tall fescue. Chlorophyll fluorescence area was found to be more reduced than chlorophyll fluorescence intensity for both acute and chronic stress experiments (Figure 3B, Figure 3C and Figure 7B, Figure 7C), indicating that chlorophyll was degraded rather than inhibited under metal stress conditions. Moreover, the microscopy results detected a statistically significant change in chlorophyll for the low dose in the chronic Cr(VI) stress experiment (Figure 7B) despite no change in bulk photosynthetic yield measurements (Figure 2). Through HCFM with MCR analysis, we discovered that Chl-a and Chl-b were reduced more than chlorophyll associated with PSI for all treated plants (Figure 5B and Figure 8B).

Unexpectedly, the MCR analysis of HCFM data identified a new broad AF signature for the moderate and severe co-stress treatments during later timepoints in the acute experiment (Figure 4 and Figure 5A). This broad AF feature has not been reported before in tall fescue but was found to be localized in globular bodies within the tissue. This spectral feature and associated localization also appeared in the chronic high Cr(VI) dose treatments at later time points (Figure 8A), indicating that it is associated with metal stress response rather than specific to co-stress treatments. There

were key differences in the fluorescence intensity and mean area of the globular bodies associated with the broad AF feature between the acute and chronic experiments (Figure 6 and Figure 9). Under acute stress, the mean area of the globular bodies increases over time for the severe co-stress condition (Figure 6C) while the number of globular bodies and mean fluorescence intensity have no trend (Figure 6B). This suggests that the globular bodies grew in size over time rather than fluorescent concentration of the cellular component associated with the broad AF feature. Under chronic Cr(VI) stress, the number of globular bodies linearly increased from day 15 to day 29 (Figure 9A). From day 15 to day 22, the broad AF mean fluorescence intensity and mean area both increased, while from day 22 to day 29, only the mean fluorescence intensity increased (Figure 9B, Figure 9C). This indicates that the globular bodies grew in size and then accumulated higher levels of the cellular component associated with the broad AF feature. Overall, these temporal trends suggest different responses to acute and chronic metal stress.

The absence of broad AF bodies in the acute Cr(VI) treatment and their appearance under the chronic high Cr(VI) dose treatment suggests that the broad AF bodies are associated with plant stress response. Based on this evidence and the spatial localization of the globular bodies, we hypothesize that the formation of the bodies may be a result of stress induced autophagy. It is known that autophagy can be induced in plants during degradation of the chloroplasts which occurs due to senescence or stress [55-57]. Further investigation is needed to determine if these bodies are a result of the autophagic process. If these bodies are identified as autophagic lysosomes, it will advance our understanding of metal stress response in tall fescue resulting from environmental metal contamination. Prior studies of autophagy in plants have focused on characterizing the proteins and genetic regulation involved in this process [55]. Visualization of autophagic bodies within plant tissue using HCFM will improve our understanding of plant autophagy at the cellular and tissue levels. Prior methods for visualizing plant autophagy include transmission electron microscopy (TEM) to detect formation and scission of the vacuolar membrane and fluorescence microscopy using autophagy-related proteins tagged with fluorescent proteins or fluorescent probes such as LysoTracker [58]. If the broad AF feature is confirmed to be associated with autophagy, HCFM and MCR analysis would provide a label-free method for visualizing plant autophagy to complement membrane visualization via TEM.

5. Conclusions

This study provides new insight to acute and chronic metal stress responses of tall fescue through both phenotypic and microscopic characterization. Under both acute and high doses of chronic metal stress, we observed common stress phenotypes, including chlorosis, necrosis, loss of leaf turgor, and reduced photosynthetic yields. HCFM with MCR analysis provided further resolution on changes in photosynthetic pigments within tall fescue after metal stress. This analysis showed greater decreases in Chl-a and Chl-b relative to chlorophyll associated with PSI for both acute and chronic metal stress treatments. A broad AF feature was also identified from MCR analysis of the HCFM datasets. This broad AF feature was localized in globular bodies under both acute (moderate and severe co-stress) and chronic (high Cr(VI) dose) metal stress treatments. Once the identity of the broad AF spectral component is confirmed, we will be able to understand the response of tall fescue more thoroughly to copper and chromium metal stress.

Acknowledgments

Sandia National Laboratories (SNL) is a multimission laboratory managed and operated by National Technology & Engineering Solutions of Sandia, LLC, a wholly owned subsidiary of Honeywell International, Inc., for the U.S. Department of Energy's National Nuclear Security Administration under contract DE-NA0003525. The authors also acknowledge Mr. Michael Howard (Nevada National Security Site), our collaborator on this project; Dr. Michael Sinclair (SNL) for his assistance in maintaining and calibrating the hyperspectral confocal fluorescence microscope; Dr. Tessily Hogancamp (SNL) and Ms. Leslie Sanford (SNL) for their assistance in acquiring the confocal fluorescence and brightfield images; and Dr. Stephen Anthony for the MATLAB scripts to determine the best focus, cell segmentation, and support of the hyperspectral analysis software.

Author Contributions

DMM and AF conducted experiments, analyzed data, and drafted the manuscript. CRS assisted with protocol development, data collection, and analysis. JBR assisted with data collection. JAT assisted with protocol development, data collection, analysis, and manuscript editing. AMR conceived the study, assisted with protocol development and data collection, and edited the manuscript. All authors have read and approved the manuscript.

Funding

This work was supported by the National Nuclear Security Administration's Office of Defense Nuclear Nonproliferation Research & Development program.

Disclaimer

This paper describes objective technical results and analysis. Any subjective views or opinions that might be expressed in the paper do not necessarily represent the views of the U.S. Department of Energy or the United States Government.

Competing Interests

The authors have declared that no competing interests exist.

Additional Materials

The following additional materials are uploaded at the page of this paper.

1. Supplemental Methods
2. Figure S1: Digital images of tall fescue for acute metal stress treatments. All treatments were applied on day 0.
3. Figure S2: Digital images of tall fescue for chronic metal stress treatments. Treatments were applied daily.
4. Figure S3: Structural measurements in tall fescue leaves. Structural features are depicted and includes leaf cross-section area (R, orange), vascular fiber bundle area (V, red), abaxial fiber bundle area (B, blue), adaxial fiber bundle area (D, yellow), metaxylem elements area (M, green), vertical

length of cross-section (L, purple), and the vertical length of cross-section sides (S, pink). Scale bar represents 50 µm.

5. Figure S4: Quantification of structural elements from brightfield microscopy images of tall fescue cross-sections for the acute metal stress experiment. (A) vein, (B) abaxial, (C) adaxial, and (D) metaxylem elements. Areas for each element were normalized by the cross-sectional area of the leaf (see Figure S3).

6. Figure S5: Illustration of how concentration maps corresponding to the abundance of each pure spectral component are merged to construct composite RGB images. Images used for this illustration are from the chronic Cr(VI) stress experiment. The colors in composite image correspond to the spectral component colors in Figure 4 with the exception of the broad AF feature: Chla = red, Chlb = green, PS1 = blue, broad AF = white. The scale bar is equal to 8 µm.

7. Figure S6: Quantification of structural elements from brightfield microscopy images of tall fescue cross-sections for the chronic metal stress experiment. (A) vein, (B) abaxial, (C) adaxial, and (D) metaxylem elements. Areas for each element were normalized by the cross-sectional area of the leaf (see Figure S3).

8. Figure S7: Quantification of relative abundances of the photosynthetic pigments Chl-a (red), Chl-b (green) and PSI (blue) across the acute metal stress experimental time course (days 0, 4, 7, and 9). All values were normalized to the control fluorescence intensity. * Designates statistical significance: * $p < 0.05$, ** $p < 0.01$, *** $p < 0.001$, **** $p < 0.0001$.

9. Figure S8: Quantification of relative abundances of the photosynthetic pigments Chl-a (red), Chl-b (green) and PSI (blue) across the chronic metal stress experimental time course (days 2, 9, 15, 22, and 29). All values were normalized to the control fluorescence intensity. * Designates statistical significance: * $p < 0.05$, ** $p < 0.01$, *** $p < 0.001$, **** $p < 0.0001$.

References

1. Proshad R, Kormoker T, Mursheed N, Islam MM, Bhuyan MI, Islam MS, et al. Heavy metal toxicity in agricultural soil due to rapid industrialization in Bangladesh: A review. Int J Adv Geosci. 2018; 6: 83-88.
2. Machender G, Dhakate R, Prasanna L, Govil P. Assessment of heavy metal contamination in soils around Balanagar industrial area, Hyderabad, India. Environ Earth Sci. 2011; 63: 945-953.
3. Hoang HG, Lin C, Tran HT, Chiang CF, Bui XT, Cheruiyot NK, et al. Heavy metal contamination trends in surface water and sediments of a river in a highly-industrialized region. Environ Technol Innov. 2020; 20: 101043.
4. He Z, Shentu J, Yang X, Baligar VC, Zhang T, Stoffella PJ. Heavy metal contamination of soils: Sources, indicators and assessment. J Environ Indic. 2015; 9: 17-18.
5. Poston TM, Hanf RW, Dirkes RL, Morasch LF. Hanford site environmental report for calendar year 2001. Richland: Pacific Northwest National Lab; 2002; PNNL-13910.
6. Hayat S, Khalique G, Irfan M, Wani AS, Tripathi BN, Ahmad A. Physiological changes induced by chromium stress in plants: An overview. Protoplasma. 2012; 249: 599-611.
7. Zachara JM, Ainsworth CC, Brown GE, Catalano JG, McKinley JP, Qafoku O, et al. Chromium speciation and mobility in a high level nuclear waste vadose zone plume. Geochim Cosmochim Acta. 2004; 68: 13-30.

8. Palmer CD, Wittbrodt PR. Processes affecting the remediation of chromium-contaminated sites. Environ Health Perspect. 1991; 92: 25-40.
9. Pandey SK. Germination and seedling growth of field pea Pisum sativum Malviya Matar-15 (HUDP-15) and Pusa Prabhat (DDR-23) under varying level of copper and chromium. J Am Sci. 2008; 4: 33-47.
10. Kotas J, Stasicka Z. Chromium occurrence in the environment and methods of its speciation. Environ Pollut. 2000; 107: 267-283.
11. Kabata-Pendia A, Pendia H. Trace elements in soils and plants. Boca Raton: CRC Press Inc; 2001.
12. Heijerick DG, Van Sprang PA, Van Hyfte AD. Ambient copper concentrations in agricultural and natural European soils: An overview. Environ Toxicol Chem. 2006; 25: 858-864.
13. Shutcha MN, Faucon MP, Kamengwa Kissi C, Colinet G, Mahy G, Ngongo Luhembwe M, et al. Three years of phytostabilisation experiment of bare acidic soil extremely contaminated by copper smelting using plant biodiversity of metal-rich soils in tropical Africa (Katanga, DR Congo). Ecol Eng. 2015; 82: 81-90.
14. Bes C, Mench M. Remediation of copper-contaminated topsoils from a wood treatment facility using in situ stabilisation. Environ Pollut. 2008; 156: 1128-1138.
15. Flores-Velez LM, Ducaroir J, Jaunet AM, Robert M. Study of the distribution of copper in an acid sandy vineyard soil by three different methods. Eur J Soil Sci. 1996; 47: 523-532.
16. Yadav SK. Heavy metals toxicity in plants: An overview on the role of glutathione and phytochelatins in heavy metal stress tolerance of plants. S Afr J Bot. 2010; 76: 167-179.
17. Gill M. Heavy metal stress in plants: A review. Int J Adv Res. 2014; 2: 1043-1055.
18. Vajpayee P, Tripathi RD, Rai UN, Ali MB, Singh SN. Chromium (VI) accumulation reduces chlorophyll biosynthesis, nitrate reductase activity and protein content in Nymphaea alba L. Chemosphere. 2000; 41: 1075-1082.
19. Ganesh KS, Baskaran L, Rajasekaran S, Sumathi K, Chidambaram AL, Sundaramoorthy P. Chromium stress induced alterations in biochemical and enzyme metabolism in aquatic and terrestrial plants. Colloids Surf B. 2008; 63: 159-163.
20. Chatterjee J, Chatterjee C. Phytotoxicity of cobalt, chromium, and copper in cauliflower. Environ Pollut. 2000; 109: 69-74.
21. Dixit V, Pandey V, Shyam R. Chromium ions inactivate electron transport and enhance superoxide generation in vivo in pea (Pisum sativum L. cv. Azad) root mitochondria. Plant Cell Environ. 2002; 25: 687-693.
22. Sharma DC, Sharma CP, Tripathi RD. Phytotoxic lesions of chromium in maize. Chemosphere. 2003; 51: 63-68.
23. Scoccianti V, Crinelli R, Tirillini B, Mancinelli V, Speranza A. Uptake and toxicity of Cr(III) in celery seedlings. Chemosphere. 2006; 64: 1695-1703.
24. Thomas JC, Malick FK, Endreszl C, Davies EC, Murray KS. Distinct responses to copper stress in the halophyte Mesembryanthemum crystallinum. Physiol Plant. 1998; 102: 360-368.
25. Lewis S, Donkin ME, Depledge MH. Hsp70 expression in Enteromorpha intestinalis (Chlorophyta) exposed to environmental stressors. Aquat Toxicol. 2001; 51: 277-291.
26. Novikova IV, Smallwood CR, Gong Y, Hu D, Hendricks L, Evans JE, et al. Multimodal hyperspectral optical microscopy. Chem Phys. 2017; 498-499: 25-32.
27. Sinclair MB, Haaland DM, Timlin JA, Jones HDT. Hyperspectral confocal microscope. Appl Opt. 2006; 45: 6283-6291.

28. Vermaas WFJ, Timlin JA, Jones HDT, Sinclair MB, Nieman LT, Hamad SW, et al. In vivo hyperspectral confocal fluorescence imaging to determine pigment localization and distribution in cyanobacterial cells. Proc Natl Acad Sci U S A. 2008; 105: 4050-4055.
29. Reddy P, Guthridge KM, Panozzo J, Ludlow EJ, Spangenberg GC, Rochfort SJ. Near-infrared hyperspectral imaging pipelines for pasture seed quality evaluation: An overview. Sensors (Basel). 2022; 22: 1981.
30. MacGregor-Chatwin C, Sener M, Barnett SFH, Hitchcock A, Barnhart-Dailey MC, Maghlaoui K, et al. Lateral segregation of photosystem I in cyanobacterial thylakoids. Plant Cell. 2017; 29: 1119-1136.
31. Ruffing AM, Jones HD. Physiological effects of free fatty acid production in genetically engineered Synechococcus elongatus PCC 7942. Biotechnol Bioeng. 2012; 109: 2190-2199.
32. Pedroso MC, Sinclair MB, Jones HD, Haaland DM. Hyperspectral confocal fluorescence microscope: A new look into the cell. Microsc Today. 2010; 18: 14-18.
33. Ball D, Lacefield G, Hoveland CS. The tall fescue endophyte. Agriculture and Natural Resources Publications; 1991. Available from: https://uknowledge.uky.edu/anr_reports/33/?utm_source=uknowledge.uky.edu%2Fanr_reports%2F33&utm_medium=PDF&utm_campaign=PDFCoverPages.
34. Peng H, Liang K, Luo H, Huang H, Luo S, Zhang A, et al. A Bacillus and Lysinibacillus sp. bio-augmented Festuca arundinacea phytoremediation system for the rapid decontamination of chromium influenced soil. Chemosphere. 2021; 283: 131186.
35. Lu M, Zhang ZZ. Phytoremediation of soil co-contaminated with heavy metals and deca-BDE by co-planting of Sedum alfredii with tall fescue associated with Bacillus cereus JP12. Plant Soil. 2014; 382: 89-102.
36. Ghadiri S, Farpoor MH, Hejazi Mehrizi M. Phytoremediation of soils polluted by heavy metals using Vetiver grass and Tall Fescue. Desert. 2018; 23: 123-132.
37. Begonia MT, Begonia GB, Ighoavodha M, Gilliard D. Lead accumulation by tall fescue (Festuca arundinacea Schreb.) grown on a lead-contaminated soil. Int J Environ Res Public Health. 2005; 2: 228-233.
38. Dong Q, Xu P, Wang Z. Differential cadmium distribution and translocation in roots and shoots related to hyper-tolerance between tall fescue and Kentucky bluegrass. Front Plant Sci. 2017; 8: 113.
39. Fei L, Xu P, Dong Q, Mo Q, Wang Z. Young leaf protection from cadmium accumulation and regulation of nitrilotriacetic acid in tall fescue (festuca arundinacea) and kentucky bluegrass (poa pratensis). Chemosphere. 2018; 212: 124-132.
40. Huang M, Ai H, Xu X, Chen K, Niu H, Zhu H, et al. Nitric oxide alleviates toxicity of hexavalent chromium on tall fescue and improves performance of photosystem II. Ecotoxicol Environ Saf. 2018; 164: 32-40.
41. Stomberg AL, Hemphill Jr DD, Volk VV, Wickliff C. Tall fescue response and soil properties following soil amendment with tannery wastes. Agron J. 1984; 76: 719-723.
42. Banks MK, Schwab AP, Henderson C. Leaching and reduction of chromium in soil as affected by soil organic content and plants. Chemosphere. 2006; 62: 255-264.
43. Shan Q, Liu X, Zhang J, Chen G, Liu S, Zhang P, et al. Analysis on the tolerance of four ecotype plants against copper stress in soil. Procedia Environ Sci. 2011; 10: 1802-1810.

44. Peterson SW, Thompson KM, Tonkin MJ. Results from recent science and technology investigations targeting chromium in the 100D area, hanford site, washington, USA. Proceedings of the WM 2010 Conference; 2010 March 7-11; Phoenix, AZ, USA. Availavle from: https://www.osti.gov/servlets/purl/968503.
45. Schindelin J, Arganda-Carreras I, Frise E, Kaynig V, Longair M, Pietzsch T, et al. Fiji: An open-source platform for biological-image analysis. Nat Methods. 2012; 9: 676-682.
46. Sadler BM, Swami A. Analysis of multiscale products for step detection and estimation. IEEE Trans Inf Theory. 1999; 45: 1043-1051.
47. Collins AM, Liberton M, Jones HDT, Garcia OF, Pakrasi HB, Timlin JA. Photosynthetic pigment localization and thylakoid membrane morphology are altered in Synechocystis 6803 phycobilisome mutants. Plant Physiol. 2012; 158: 1600-1609.
48. Jones HD, Haaland DM, Sinclair MB, Melgaard DK, Collins AM, Timlin JA. Preprocessing strategies to improve MCR analyses of hyperspectral images. Chemom Intell Lab Syst. 2012; 117: 149-158.
49. Haaland DM, Jones HDT, Van Benthem MH, Sinclair MB, Melgaard DK, Stork CL, et al. Hyperspectral confocal fluorescence imaging: Exploring alternative multivariate curve resolution approaches. Appl Spectrosc. 2009; 63: 271-279.
50. Banks MK, Schwab AP, Henderson C. Leaching and reduction of chromium in soil as affected by soil organic content and plants. Chemosphere. 2006; 62: 255-264.
51. Huang M, Ai H, Xu X, Chen K, Niu H, Zhu H, et al. Nitric oxide alleviates toxicity of hexavalent chromium on tall fescue and improves performance of photosystem II. Ecotoxicol Environ Saf. 2018; 164: 32-40.
52. Stomberg AL, Hemphill Jr DD, Volk VV, Wickliff C. Tall fescue response and soil properties following soil amendment with tannery wastes. Agron J. 1984; 76: 719-723.
53. Panda S, Choudhury S. Chromium stress in plants. Braz J Plant Physiol. 2005; 17: 95-102.
54. Yruela I. Copper in plants: Acquisition, transport and interactions. Funct Plant Biol. 2009; 36: 409-430.
55. Su T, Li X, Yang M, Shao Q, Zhao Y, Ma C, et al. Autophagy: An intracellular degradation pathway regulating plant survival and stress response. Front Plant Sci. 2020; 11: 164.
56. Zhuang X, Jiang L. Chloroplast degradation: Multiple routes into the vacuole. Front Plant Sci. 2019; 10: 359.
57. Jiang Z, Zhu L, Wang Q, Hou X. Autophagy-related 2 regulates chlorophyll degradation under abiotic stress conditions in arabidopsis. Int J Mol Sci. 2020; 21: 4515.
58. van Doorn WG, Papini A. Ultrastructure of autophagy in plant cells: A review. Autophagy. 2013; 9: 1922-1936.

Enjoy *AEER* by:

1. Submitting a manuscript
2. Joining in volunteer reviewer bank
3. Joining Editorial Board
4. Guest editing a special issue

For more details, please visit:
http://www.lidsen.com/journals/aeer